

An illusion predicted by V1 population activity implicates cortical topography in shape perception

Melchi M Michel¹, Yuzhi Chen²⁻⁴, Wilson S Geisler^{2,3} & Eyal Seidemann²⁻⁴

Mammalian primary visual cortex (V1) is topographically organized such that the pattern of neural activation in V1 reflects the location and spatial extent of visual elements in the retinal image, but it is unclear whether this organization contributes to visual perception. We combined computational modeling, voltage-sensitive dye imaging (VSDI) in behaving monkeys and behavioral measurements in humans to investigate whether the large-scale topography of V1 population responses influences shape judgments. Specifically, we used a computational model to design visual stimuli that had the same physical shape, but were predicted to elicit variable V1 response spread. We confirmed these predictions with VSDI. Finally, we designed a behavioral task in which human observers judged the shapes of these stimuli and found that their judgments were systematically distorted by the spread of V1 activity. This illusion suggests that the topographic pattern of neural population responses in visual cortex contributes to visual perception.

Humans are remarkably sensitive to differences in the sizes and shapes of visual objects. For example, we can detect small deviations from circularity and subtle differences in the aspect ratios of different shapes and we can make these discriminations over a wide range of image sizes, regardless of whether the shapes are defined by texture, disparity or luminance boundaries¹⁻³. Researchers have postulated a variety of local^{4,5} and global^{2,6} mechanisms to explain the human ability to perceive particular shape stimuli. An often implicit assumption in these models is that human observers have access to a spatial distribution of filter outputs modeled on the response properties of V1 neurons. The spatial distributions of these neural responses in primate V1 have been measured using various techniques⁷⁻¹². At a sub-millimeter scale, V1 population responses are organized into orientation columns, such that the receptive fields of neighboring neurons share similar orientation preferences. At a larger spatial scale, the responses are organized retinotopically, with nearby neurons representing neighboring locations in the visual field. Although this organization is serendipitous for researchers investigating the properties of cortical neurons (for example, by making it relatively easy to locate neurons that code for similar visual properties), its role in perception is unclear and the functional relevance of such topographical maps remains an active topic of debate¹³⁻¹⁷.

One hypothesis is that these topographical maps may simply be epiphenomena of cortical development, with little functional relevance for neural coding and perception¹³. In this view, perceptual judgments might be implemented by flexible decoding mechanisms that combine responses of cortical neurons in a way that is insensitive to their location in the topographic map. Indeed, by ignoring local cortical topography entirely, several prominent models of optimal

neural decoding implicitly assume this hypothesis¹⁸⁻²⁰. The strong version of this 'labeled line' hypothesis asserts that the decoding circuits take into account the specific tuning properties of each neuron in the population (for example, the position, peaks and bandwidths of orientation and spatial frequency tuning).

An alternative hypothesis is that the decoding circuits exploit cortical topography^{14,21,22}. In the strong version of this hypothesis, the decoder pools all neurons at the same topographic location while ignoring their specific tuning properties. For example, local pooling of responses at each of the two topographic scales described above might subserve different sets of visual judgments (Fig. 1). Signals at the orientation-column scale pool responses across neurons with similar orientation tuning and reflect the fine-scale orientation content of the visual stimulus, providing information that might be used primarily for discriminating between, or identifying, visual textures. Signals at the retinotopic scale pool responses across neurons with similar location tuning and might be used primarily for computing the locations, shapes and sizes of visual objects.

If the visual system is exploiting V1 topography, then stimulus-dependent distortions in the topographic representation may result in concomitant perceptual distortions. On the other hand, if the visual system exclusively uses a labeled line decoder, then there is no reason to expect that topographic distortions would affect perception (see Discussion). To test the hypothesis that V1 topography is involved in shape coding, we first used a model of V1 population responses, combined with VSDI, to find stimuli with equal physical shape, but different topographic representations in V1. We found that these stimuli produced the perceptual distortions expected if the topographic representation in V1 contributed to shape perception.

¹Department of Psychology, Rutgers University, New Brunswick, New Jersey, USA. ²Center for Perceptual Systems, University of Texas at Austin, Austin, Texas, USA. ³Department of Psychology, University of Texas at Austin, Austin, Texas, USA. ⁴Section of Neurobiology, University of Texas at Austin, Austin, Texas, USA. Correspondence should be addressed to M.M.M. (melchi.michel@rutgers.edu).

Received 3 April; accepted 18 August; published online 15 September 2013; doi:10.1038/nn.3517

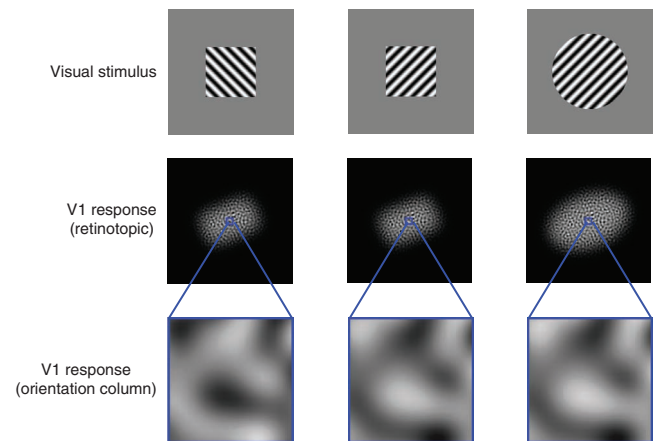
Figure 1 Schematic illustration of two scales of functional organization in primary visual cortex. The top row shows texture-defined visual shapes that differ either in terms of the textures that define them (left and center columns) or their shape (center and right columns). The middle row schematically illustrates retinotopic-scale V1 population responses to the visual stimuli. The spatial spread or retinotopic extent of activation at this scale can be used to discriminate between the sizes and coarse shapes of visual stimuli, but not to discriminate between their component textures. The bottom row shows schematic responses in orientation columns. Signals at this scale can be used to distinguish between the orientation content of component textures, but not to determine the global shapes of the visual stimuli.

RESULTS

Simulating V1 population responses

To simulate the expected retinotopic extent of V1 population responses, we created a large population of model V1 neurons representing a $2^\circ \times 2^\circ$ patch of the visual field (centered 3° from the fovea) and having realistic distributions of orientation, spatial frequency and size tuning (**Supplementary Fig. 1**). The model predicts that, for most visual stimuli, the retinotopic extent of V1 population activity, pooled locally at the retinotopic scale, provides a reliable signal for shape judgment. However, we found that, for a small subset of stimuli, the retinotopic extent of V1 activity could be dissociated from the physical shape of the stimulus. Specifically, the model predicts that small sine-wave stimuli (Gabor) with a circular contrast envelope and spatial frequency and size similar to that of the average V1 neuron's receptive field should produce a retinotopic pattern of population activity that is systematically extended in the direction of grating (the carrier) orientation. This effect results from the tendency of V1 receptive fields to be elongated along the direction of their preferred orientation^{23–25}.

A consequence of this elongation is that neurons will tend to respond at greater distances to stimuli collinearly aligned with their receptive fields than to stimuli aligned orthogonally, yielding a



population response that is retinotopically elongated along the orientation of the carrier (**Fig. 2a–d**). This orientation-dependent distortion disappears if the spatial frequency or spatial frequency bandwidth of the Gabor stimulus is sufficiently different from the optimal value (**Fig. 2c,e**) or if the stimulus contains multiple orientation components. Thus, if the predictions of our model are correct, and if the extent of the spread of activity in the retinotopic map of V1 influences perceptual estimates of visual shape, the perceived stimulus aspect ratio should be systematically distorted by carrier orientation for stimuli that approximately match the average V1 receptive field.

Imaging orientation-dependent V1 response spread

To confirm that V1 population responses exhibit this orientation-dependent elongation, we measured V1 population responses in awake, fixating macaques using VSDI, which is uniquely well-suited to the investigation of large-scale population activity and cortical topography²⁶. Using VSDI responses from 17 recording sessions in three monkeys, we found that the carrier orientation systematically altered the retinotopic extent of population responses in V1, as predicted by our model. Note that, as the retinotopic map in V1 is locally contiguous, we can express the retinotopy of a small patch of the cortical surface as an isomorphic transformation of a small patch of the visual field. We measured the coarse retinotopy of the

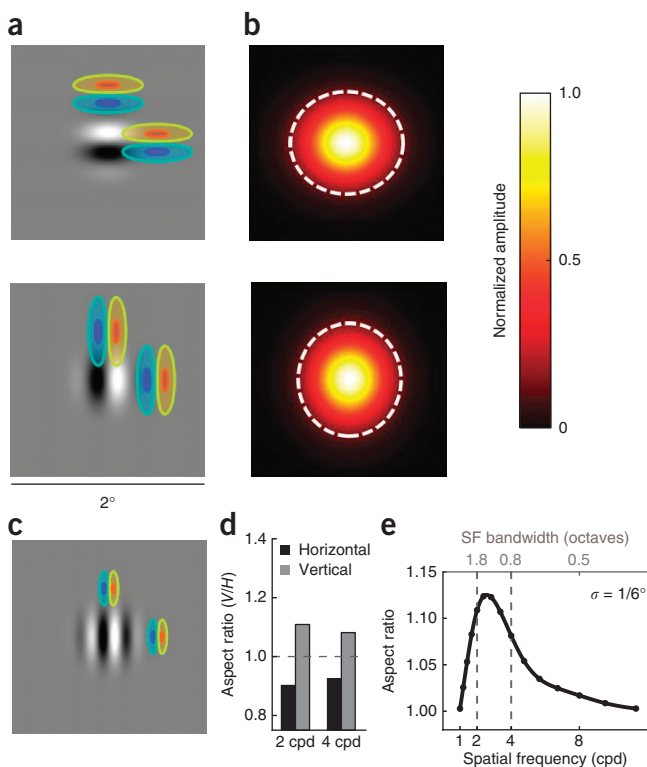
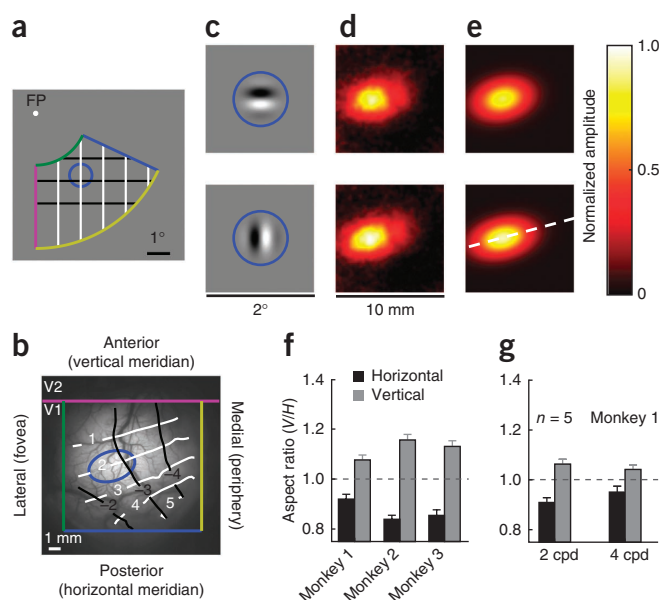


Figure 2 Predicted effects of elongated receptive fields on the spatial distribution of V1 population responses. **(a)** Receptive fields (overlaid contours) well-tuned to a stimulus (grayscale image) and displaced by equal distances in collinear and orthogonal directions. The stimulus overlaps more with collinearly than orthogonally displaced receptive fields, eliciting cortical population responses elongated along the direction of the Gabor orientation. **(b)** Population responses predicted for the 2-cpd Gabors depicted in **a** using a retinotopic V1 model, shown in visual field coordinates. The dashed white ellipses indicate the 3σ contour of a Gaussian fitted to the population response. For a simulated population of neurons with receptive field parameters based on physiological measurements, the population response is elongated along the direction of carrier orientation. **(c)** Effect of carrier spatial frequency on cortical response elongation. Because receptive field size is inversely correlated with peak spatial frequency⁴³, increasing spatial frequency leads to activation of neurons with smaller receptive fields, reducing the effect of receptive field elongation on the cortical response. **(d)** Response aspect ratios predicted by the V1 model for 2-cpd (left) and 4-cpd (right) Gabor stimuli with vertical (V) and horizontal (H) carriers. **(e)** Predicted response distortion as a function of carrier spatial frequency for a Gabor with a fixed envelope size ($\sigma = 0.167^\circ$). The abscissa at the top of the panel indicates the spatial frequency (SF) bandwidths of the Gabor stimuli, and the dashed lines represent stimuli used in the physiological experiments.

Figure 3 Physiological stimuli and spatial distributions of V1 responses measured with VSDI. (a) Schematic of the visual field with $1^\circ \times 1^\circ$ rectangular grid. The colored lines represent the approximate limits of visual space in our imaging window, and the solid blue circle represents the 3σ contour of the stimulus envelope. (b) Image of the cortical vasculature in one of our chambers (monkey 1, left hemisphere) with overlaid scale marker, landmarks and retinotopy. The blue ellipse represents the approximate retinotopic contours of the circle in a. The white and black curves represent the vertical and horizontal gridlines in a. (c) The visual stimuli, with solid blue circles overlaid to indicate the 3σ contour of the stimulus envelopes for the horizontal (top) and vertical (bottom) Gabor stimuli. (d) Amplitudes of cortical responses in a $10 \times 10 \text{ mm}^2$ patch of cortex to the horizontal (top) and vertical (bottom) Gabor stimuli, averaged over an experimental session. (e) Two-dimensional Gaussian fits to the responses in d. The dashed white line represents a vertical line in the visual field located 2 degrees to the right of fixation. Relative to the retinotopic shape of the stimulus (blue ellipse in b), the vertical Gabor is vertically elongated and the horizontal Gabor is horizontally elongated. (f) Normalized aspect ratios ($AR_{\text{response}}/AR_{\text{retinotopic}}$) of responses to 2-cpd horizontal and vertical Gabors measured in three different monkeys, demonstrating both the robustness of the orientation-dependent elongation effect and the variability of its magnitude across different individuals ($n = 5$ experiments for monkey 1, 8 experiments for monkey 2, and 4 experiments for monkey 3). (g) Normalized population response aspect ratios obtained in one chamber for spatial frequencies of 2 cpd and 4 cpd (monkey 1, $n = 5$ experiments). Error bars represent 95% confidence intervals.



cortical surface in our recording chambers (Fig. 3). It should be noted that a circle in the visual field (Fig. 3a) projects to an ellipse on the surface of the cortex (Fig. 3b). This is a result of the well-documented anisotropy in cortical magnification parallel versus perpendicular to the V1/V2 border^{7,8,10,12,22}. We were not interested in this anisotropy, which represents a fixed mapping from the visual field to the cortical surface. Rather, we were interested in determining whether varying the carrier orientation of a fixed-envelope Gabor stimulus results in population responses whose cortical extent varies systematically relative to this fixed mapping. The visual stimuli (Fig. 3c) were small Gabor patches composed of a vertically or horizontally oriented carrier grating windowed by a circularly symmetric Gaussian envelope. To quantify the spatial spread of the response to each stimulus, we computed the s.d. parameters of an elliptical two-dimensional Gaussian function fit (Fig. 3e) to the average response amplitudes (Fig. 3d).

Although the spatial extents of the horizontally and vertically oriented Gabors in the visual field were identical, the spread of the cortical responses varied systematically with the carrier orientation (Fig. 3d–g).

Responses to the vertical Gabor were elongated along the cortical direction corresponding to the vertical axis in the visual field (Fig. 3e) and shortened along the orthogonal direction ($AR_V/\overline{AR} = 1.12$, one-sample $t_{16} = 175.73$, $P = 1.02 \times 10^{-27}$, where AR_V , AR_H and \overline{AR} represent the vertical-to-horizontal retinotopic aspect ratios of the horizontal and vertical Gabors and their mean, respectively), whereas responses to the horizontal Gabor were elongated along the cortical direction corresponding to horizontal and shortened along the vertical direction ($AR_H/\overline{AR} = 0.87$, one-sample $t_{16} = 158.09$, $P = 5.51 \times 10^{-27}$). Experiments using additional stimuli (Fig. 4) confirmed that these systematic changes in the retinotopic-scale population responses reflected the effect of the carrier orientation. For example, the responses to plaid and Gaussian stimuli, which contain energy at both the vertical and horizontal orientations, exhibited no systematic retinotopic distortion (Fig. 4a); the vertical-to-horizontal aspect ratio of elicited responses varied systematically as a function of carrier orientation, with responses to horizontal orientations exhibiting the smallest aspect ratios and those to vertical orientations exhibiting the largest aspect ratios (Fig. 4b).

Figure 4 Spatial properties of physiological responses for additional stimuli. (a) Normalized vertical-to-horizontal aspect ratio of VSDI response to stimuli with an identical, circular Gaussian contrast envelope with a 2-cpd horizontal, vertical, plaid or luminance carrier (Gauss). In contrast to the horizontal and vertical Gabors, population responses to the plaid and Gaussian stimuli did not exhibit retinotopic elongation. (b) Normalized vertical-to-horizontal aspect ratio of responses to 2-cpd carriers with orientations spaced at 30° intervals. As expected, the vertical-to-horizontal aspect ratio was largest for vertical stimuli (90°), smallest for horizontal stimuli (0°) and varied smoothly across intermediate orientations. (c) Model predictions (curves) and measurements (circles; $n = 2$ experimental sessions) of the orientation-dependent elongation effect, measured as the differences between the aspect ratios of responses to vertically (AR_V) and horizontally (AR_H) oriented Gabor stimuli as a function of spatial frequency for different Gaussian envelope sizes (σ). The observed effects of varying envelope size and spatial frequency are qualitatively consistent with those predicted by the model. Data in all panels are from monkey 1. Error bars represent 95% confidence intervals.

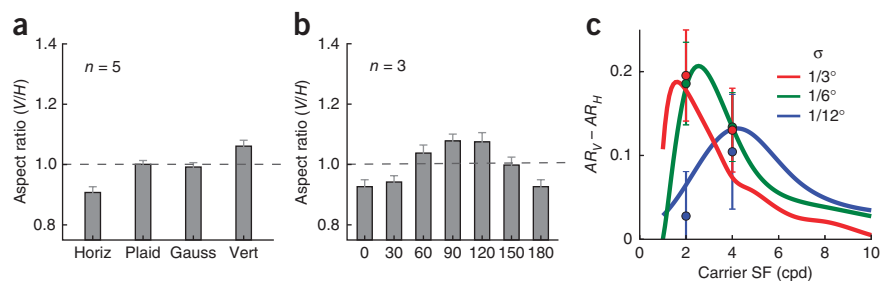
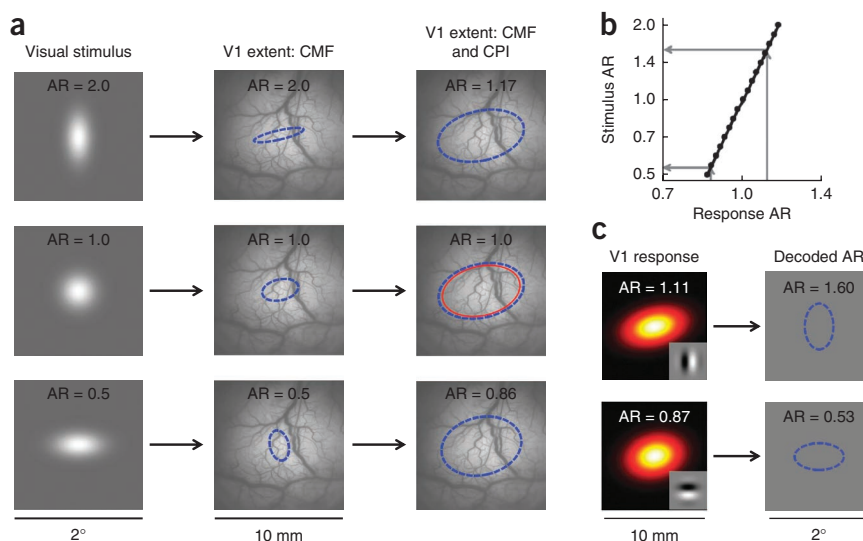


Figure 5 Modeling the relationship between the spatial extent of a visual stimulus and the retinotopic extent of its elicited cortical response. **(a)** A schematic representation of the cortical responses to vertical (top), isotropic (middle) and horizontal (bottom) Gaussian stimuli. The first column shows the visual stimulus, the second column illustrates the mapping resulting from the fixed retinotopic projection to V1 (**Fig. 3b**), which can be expressed in terms of the local CMF, and the third column illustrates the added effect of the CPI, whose size is indicated by the thin red ellipse in the central row. The dashed blue ellipses represent the 2σ Gaussian envelope contours of the predicted VSDI responses. Retinotopic aspect ratios (ARs) are indicated at the top of each image. **(b)** Predicted aspect ratio of a Gaussian stimulus as a function of the retinotopic aspect ratio of its elicited response. As a result of the large size of the CPI relative to the retinotopic extent of the visual stimuli, the aspect ratio of the elicited cortical response

is retinotopically compressed, with an envelope that tends to be more isotropic than that of the eliciting stimulus. **(c)** Perceptual orientation-dependent elongation predicted by the V1 model for the 2-cpd vertical (top) and horizontal (bottom) circular Gabor stimuli if observers compensate for the effects of the aspect ratio compression shown in **b**. The dashed blue ellipses represent the predicted 2σ Gaussian envelope contour of the perceived stimulus.



A key prediction of our model was that the orientation-dependent distortions should diminish as the stimulus' spatial frequency or spatial frequency bandwidth deviate from the optimal values (**Fig. 2c,e**). To test this prediction, we ran additional conditions with suboptimal Gabor stimuli with identical envelopes, but double the spatial frequency. For all stimuli, the VSDI response was still elongated in the direction corresponding to the Gabor's carrier orientation (**Fig. 3g**). However, as predicted, the difference between the aspect ratios of the responses to horizontal and vertical Gabors was significantly smaller for the higher spatial frequency stimuli ($(AR_V - AR_H)/\overline{AR} = 0.09$) than for the lower spatial frequency stimuli ($(AR_V - AR_H)/\overline{AR} = 0.15$; paired $t_4 = 5.34$, $P = 0.006$).

To further test the predictions of our model, we created several additional stimulus conditions by doubling or halving the size of the Gaussian contrast envelope while keeping the carrier spatial frequencies at 2 and 4 cpd. The model predicted that, for Gabor stimuli with envelope sizes (σ) of $1/3^\circ$ and $1/6^\circ$, increasing the carrier spatial frequency from 2 to 4 cpd would attenuate the elongation effect, whereas, for Gabor stimuli with an envelope size of $1/12^\circ$, increasing the carrier spatial frequency would enhance the elongation effect. Across these stimulus conditions, the patterns of elicited VSDI response aspect ratios were qualitatively consistent with the predictions of our V1 population response model (**Fig. 4c**). Overall, our physiological results confirm the hypothesis that, as a result of receptive field elongation, the retinotopic-scale topography of V1 population responses can be distorted systematically by the orientation of local visual features.

Perceptual consequences: a shape illusion

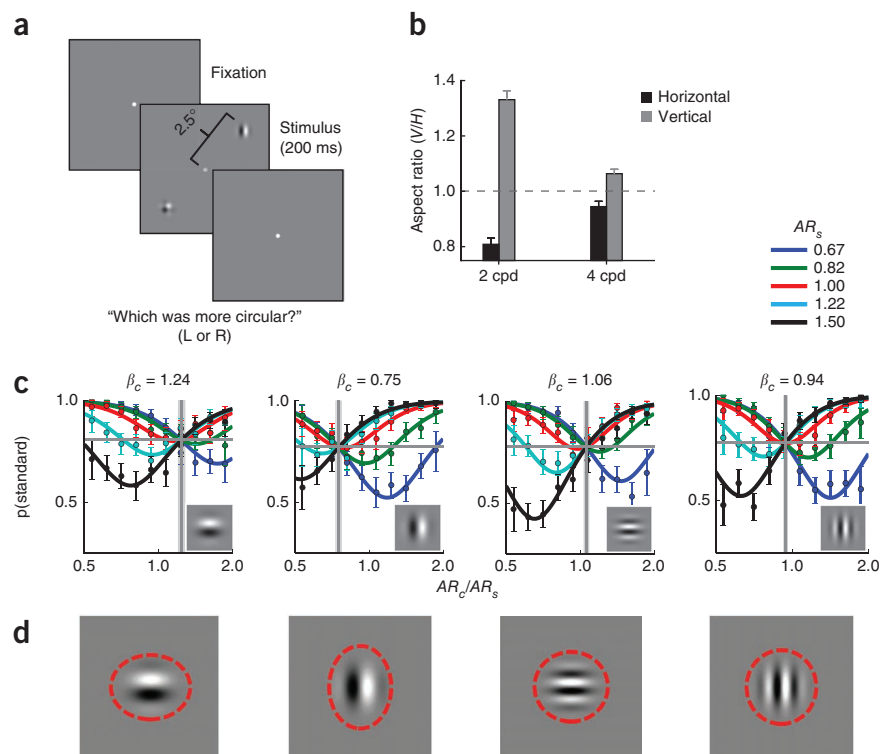
Our primary goal was to test the hypothesis that the retinotopic extent of V1 activation influences shape perception. If this hypothesis is correct, then the circuits that estimate shape on the basis of the V1 activation pattern must take into account the mapping between the retinotopic extent of V1 activation and the shape of the visual stimulus. Thus, our next step was to characterize this mapping. To do this, we first focused on stimuli that do not produce the orientation-dependent distortion.

The cortical spread of the response elicited by a visual stimulus depends on both its direct retinotopic mapping (**Fig. 3a,b**), which can be described in terms of the local cortical magnification factor (CMF)²⁷, and on the cortical point image (CPI), which describes the shape and size of the cortical surface in V1 that processes information from a single point in visual space^{28,29}. To determine the expected cortical spread as a function of visual spatial extent, we used our model, together with our VSDI-based estimates of the CMF and CPI, to predict the cortical response spread to Gaussian stimuli with aspect ratios ranging from 0.5 to 2.0 (**Fig. 5a**). The Gaussian stimuli had an average space constant equal to that of our Gabor stimuli ($1/6^\circ$). As a result of the large size of the CPI relative to the direct retinotopic projection of the stimuli, the aspect ratios of the predicted cortical responses were considerably smaller than the aspect ratios of the visual stimuli (**Fig. 5a**). In other words, for these small stimuli, large deviations from spatial isotropy in the visual field are associated with considerably smaller deviations from retinotopic isotropy in the cortical response. This systematic cortical aspect ratio compression is further illustrated in **Figure 5b**, which shows the relationship between the retinotopic aspect ratio of the cortical response and the aspect ratio of the Gaussian visual stimulus.

To accurately estimate the stimulus' aspect ratio from the cortical response aspect ratio, shape decoding mechanisms must take this relationship into account. Consider decoding the cortical responses to circular Gabor patches with horizontal and vertical carriers (**Fig. 3c-g**). If the decoding mechanisms are exploiting the relationship between spatial and retinotopic aspect ratios (**Fig. 5b**), then the estimated visual aspect ratios (**Fig. 5c**) should be much larger than the retinotopic aspect ratios that we observed physiologically. Specifically, a circular Gabor with a vertical carrier should have a perceived aspect ratio of 1.6, whereas a circular Gabor with horizontal carrier should have a perceived aspect ratio of 0.57. We hypothesized that such Gabor stimuli might produce a visual illusion, with small circular Gabors appearing stretched in the direction corresponding to the orientation of their carrier gratings.

We tested this hypothesis in human observers by designing a suitable psychophysical task (**Fig. 6a**). Testing this hypothesis in human

Figure 6 Psychophysical results averaged across ten subjects. **(a)** Schematic of the visual stimulus. Human observers briefly (200 ms) viewed a display consisting of a plaid standard and an oriented comparison stimulus whose vertical-to-horizontal aspect ratios were selected randomly, and were asked to decide which stimulus had a more circular envelope. **(b)** Psychophysically determined perceptual aspect ratios and 95% confidence intervals for 2-cpd and 4-cpd Gabor stimuli ($n = 10$ human subjects). **(c)** Psychometric functions obtained for horizontal and vertical 2-cpd and 4-cpd comparison Gabors. The abscissae represent the relative aspect ratio of the comparison stimuli ($AR_{\text{comparison}}/AR_{\text{standard}}$) and the ordinates represent the probability of selecting the standard as more circular. Each of the solid curves represents the psychometric function for a particular standard aspect ratio. The colored markers represent the corresponding observed response probabilities and 95% confidence intervals averaged across each of ten aspect ratio bins. In each plot, the horizontal gray line represents γ , the estimated guess rate, and the vertical gray line and shaded region represent the estimated point of subjective equality (PSE), which corresponds to the reciprocal of the perceived aspect ratio, and its 95% confidence interval, respectively. The comparison stimulus is indicated by the inset images. **(d)** The Gabor comparison stimuli at an aspect ratio of 1.0. The dashed red ellipses illustrate the perceived shapes of these stimuli as estimated by the PSEs. Error bars represent 95% confidence intervals.



subjects had two advantages: it allowed us to avoid methodological confounds that can arise when training monkeys to make subjective judgments in visual illusions and it allowed us to minimize possible learning effects by omitting performance feedback. Observers briefly viewed a display containing two stimulus patches on opposite sides of the screen. One of the patches, the standard, was a composite Gabor stimulus (a plaid) composed of both horizontally and vertically oriented gratings. This plaid patch acted as a neutral stimulus. The other patch, the comparison, was a simple Gabor containing either a vertical or a horizontal grating. In each trial, the vertical-to-horizontal aspect ratio of the Gaussian contrast envelope defining each of the two patches was chosen randomly and observers were asked to judge which of the patches appeared more circular (Online Methods).

Thus, each trial requires the observer to compare the aspect ratios of a (neutral) plaid stimulus and an oriented Gabor stimulus. If, as hypothesized, the oriented Gabors are perceived as being more elongated along their carrier orientation than the neutral plaids, then, for a Gabor's aspect ratio to appear equal to that of a plaid stimulus, the Gabor has to be stretched in the direction orthogonal to its carrier orientation. For example, to match the perceived shape of a plaid with a vertical-to-horizontal aspect ratio of 1, a vertical Gabor would need to have an aspect ratio smaller than 1, whereas a horizontal Gabor would need to have an aspect ratio larger than 1.

The results of our psychophysical experiments confirmed these predictions and suggest a previously unknown shape illusion. Psychometric functions (Fig. 6b) were estimated for each of five different standard aspect ratios ($AR_s = \{0.67, 0.82, 1.0, 1.22, 1.5\}$). As predicted, across all values of the standard, human observers perceived the horizontal Gabor to be horizontally stretched ($AR_H = 0.81$, one-sample $t_9 = 68.76$, $P = 1.47 \times 10^{-13}$) and the vertical Gabor to be vertically stretched ($AR_V = 1.33$, one-sample $t_9 = 81.18$, $P = 3.31 \times 10^{-14}$)

relative to the plaid stimulus. These perceived shape distortions are consistent with, but somewhat smaller than, predictions based on the physiological data (Fig. 5c). This difference was not unexpected. Although we expected qualitative agreement between the monkey physiology and the human psychophysics, multiple factors make it difficult to make precise quantitative predictions about perceptual judgments on the basis of our physiological measurements (Online Methods).

As in the physiological portion of the study, we expected the perceptual distortion to decrease for stimuli that poorly matched V1 receptive fields. To test this prediction, we ran additional psychophysical conditions using Gabor stimuli with identical Gaussian envelope sizes, but double the spatial frequency. As predicted, the perceived difference in the aspect ratios of vertical and horizontal Gabors was significantly smaller for the higher spatial frequency Gabors ($AR_V - AR_H = 0.12$) than for the lower spatial frequency Gabors ($AR_V - AR_H = 0.49$; paired $t_9 = 29.42$, $P = 2.96 \times 10^{-10}$; Fig. 6b–d). Overall, our psychophysical results indicate that, for small stimuli with oriented texture, human observers exhibit shape judgment biases consistent with those predicted by the topographical distortions observed in V1 population responses.

DISCUSSION

Visual stimuli elicit widespread activation in V1 as a result of their overlap with the receptive fields of many V1 neurons^{9,27–29}. Generally, the retinotopic extent of this activation is dominated by the spatial extent of the stimulus and should therefore serve as a reliable signal for size and shape judgments. However, we found that, for small visual stimuli dominated by a single texture orientation, this activation extended farther in the direction collinear with the texture orientation than in the orthogonal direction, leading to a distorted

pattern of retinotopic activation that varied systematically with texture orientation. We exploited this orientation-dependent distortion to test the hypothesis that human observers rely (at least in part) on the retinotopic extent of population activity in V1 when making shape judgments. Our behavioral results support this hypothesis. In addition, our results provide a rare example of a perceptual illusion predicted from new physiological observations.

As our modeling results suggest, the orientation-dependent distortion at the population level can be explained by the previously documented elongation of receptive fields in V1. Given this receptive field elongation, one's first intuition may be that the perceptual illusion reported here would be predicted by any decoder, including labeled line decoders. However, this is not the case. It is well known from sampling theory that there are many receptive field encoding schemes (including those with elongated receptive fields) that will preserve all the information in an image, and therefore allow a labeled line decoder to extract image properties without loss or distortion. Thus, there is no a priori reason to expect a labeled line decoder to be affected by receptive field elongation. It is possible to postulate *post hoc* a labeled line decoder that ignores this fundamental receptive-field property, but such a decoder is bound to make systematic errors for a wide range of visual stimuli, not just the very specific stimuli that produce a distortion in the retinotopic pattern of activity. This seems unlikely given the veridicality of shape perception under most circumstances. Thus, the most parsimonious explanation of our results is that the retinotopic pattern of activity contributes to shape perception, at least for the stimuli in our study.

Our results suggest that cortical topography is one factor influencing shape perception, but not that it is the only such factor. In fact, it is likely that a variety of mechanisms, including mechanisms that are more consistent with a labeled line hypothesis, contribute to shape perception.

Why do human observers not compensate for the retinotopically distorted responses elicited by our Gabor stimuli? After all, the cortical map exhibits many distortions and inhomogeneities, both at a fine scale, where position-based maps give way to orientation and ocular dominance-based maps, and at a coarser scale, where the area of cortex devoted to different regions of visual space varies systematically. For example, near the V1/V2 border, the cortical magnification was considerably smaller in the horizontal direction than in the vertical direction (Fig. 3a,b). Nonetheless, observers did not seem to exhibit a corresponding perceptual bias, perceiving visual space to be compressed in the horizontal direction. Similarly, observers appeared to have veridical shape perception for most small visual stimuli despite their aspect ratio compression in V1 (Fig. 5a,b). Two important differences separate these distortions from those elicited by our oriented Gabors. First, unlike the fixed spatial distortions in the V1 retinotopic map or the fixed aspect ratio compression, the distortions introduced by our stimuli vary as a function of the stimulus' carrier (that is, texture) orientation. Second, as with most visual illusions, these distortions only occur for a small, carefully selected subset of stimuli. Thus, although the shape distortions elicited by these oriented Gabor stimuli reveal an important feature of the visual mechanisms mediating shape perception, they are unlikely to systematically bias the shape judgments humans make in natural tasks.

In addition to their importance regarding shape perception, the observed orientation-dependent distortions of V1 response spread could have implications for the representation of multiple contour elements in V1. Physiological^{5,30} and psychophysical^{31,32} studies have shown that nearby collinear elements tend to have stronger interactions than orthogonal elements at the same distance. Our findings

suggest that some of these effects could result from the elongation of V1 population responses along the retinotopic representation of contour orientation. As a result of this elongation, V1 representations of two collinear elements will have larger overlap than the representations of two orthogonal elements at the same distance. Additional studies will be needed to determine the exact contribution of this elongation to collinear interactions in V1.

Researchers have previously reported relationships between perception and the retinotopic extent of V1 activation^{33–36}. For example, the surface area of V1 or of a portion of V1 can predict the ability of individual human observers to accurately report the relative positions³³ or relative sizes³⁴ of visual stimuli, suggesting that stimuli encoded using larger neural populations may be perceptually represented with greater fidelity. Other studies^{35,36} found that, in the context of a configural size illusion, attention can act to correlate the retinotopic extent of activation in V1 with the (erroneous) perceived size of visual stimuli, suggesting that the extent of activation in V1 may reflect perceived size. Our findings go beyond these previous results by demonstrating that human shape perception can be biased by stimuli that are coextensive in visual space, but vary in the retinotopic extent of their elicited activation in V1. More generally, our results suggest that the retinotopic pattern of population responses in V1 might influence, or constrain, shape perception. This finding is consistent with recent reports^{37,38} that later visual areas, which have been more directly implicated in shape processing^{39–42}, seem to sample from an approximately constant extent of the V1 cortical surface, thereby inheriting the retinotopic inhomogeneities of V1. In conclusion, our results suggest that the retinotopic extent of population activity in V1 influences human shape judgments. Thus, our findings support the hypothesis that cortical topography is important for sensory coding and for supporting perceptual judgments.

METHODS

Methods and any associated references are available in the [online version of the paper](#).

Note: Any Supplementary Information and Source Data files are available in the online version of the paper.

ACKNOWLEDGMENTS

We thank T. Cakic and other members of the Seidemann laboratory for their contributions to this project. This work was supported by grants from the National Eye Institute (R01EY016454 and R01EY16752 to E.S., and R01EY02688 and R01EY110747 to W.S.G.).

AUTHOR CONTRIBUTIONS

All of the authors contributed to the design of the study and the planning of the analysis. M.M.M. designed the V1 population response model and performed the analysis. Y.C. and E.S. performed the physiological experiments. M.M.M. performed the psychophysical experiments. M.M.M., W.S.G. and E.S. wrote the paper with input from Y.C.

COMPETING FINANCIAL INTERESTS

The authors declare no competing financial interests.

Reprints and permissions information is available online at <http://www.nature.com/reprints/index.html>.

1. Regan, D., Hajdur, L.V. & Hong, X. Two-dimensional aspect ratio discrimination for shape defined by orientation texture. *Vision Res.* **36**, 3695 (1996).
2. Regan, D. & Hamstra, S.J. Shape discrimination and the judgment of perfect symmetry: dissociation of shape from size. *Vision Res.* **32**, 1845 (1992).
3. Regan, D. & Hamstra, S.J. Shape discrimination for rectangles defined by disparity alone, by disparity plus luminance and by disparity plus motion. *Vision Res.* **34**, 2277 (1994).
4. Field, D.J., Hayes, A. & Hess, R.F. Contour integration by the human visual system: evidence for a local "association field". *Vision Res.* **33**, 173 (1993).

5. Kapadia, M.K., Ito, M., Gilbert, C.D. & Westheimer, G. Improvement in visual sensitivity by changes in local context: parallel studies in human observers and in V1 of alert monkeys. *Neuron* **15**, 843 (1995).
6. Wilson, H.R. & Wilkinson, F. Detection of global structure in Glass patterns: implications for form vision. *Vision Res.* **38**, 2933 (1998).
7. Adams, D.L. & Horton, J.C. A precise retinotopic map of primate striate cortex generated from the representation of angioscotomas. *J. Neurosci.* **23**, 3771 (2003).
8. Blasdel, G. & Campbell, D. Functional retinotopy of monkey visual cortex. *J. Neurosci.* **21**, 8286 (2001).
9. Hubel, D.H. & Weisel, T. Functional architecture of macaque monkey visual cortex. *Proc. R. Soc. Lond. B Biol. Sci.* **198**, 1 (1977).
10. Tootell, R.B., Switkes, E., Silverman, M.S. & Hamilton, S.L. Functional anatomy of macaque striate cortex. II. Retinotopic organization. *J. Neurosci.* **8**, 1531 (1988).
11. Wandell, B.A., Dumoulin, S.O. & Brewer, A.A. Visual field maps in human cortex. *Neuron* **56**, 366 (2007).
12. Yang, Z., Heeger, D.J. & Seidemann, E. Rapid and precise retinotopic mapping of the visual cortex obtained by voltage-sensitive dye imaging in the behaving monkey. *J. Neurophysiol.* **98**, 1002 (2007).
13. Horton, J.C. & Adams, D.L. The cortical column: a structure without a function. *Philos. Trans. R. Soc. Lond. B Biol. Sci.* **360**, 1837 (2005).
14. Chklovskii, D.B. & Koulakov, A.A. Maps in the brain: what can we learn from them? *Annu. Rev. Neurosci.* **27**, 369 (2004).
15. Paik, S.-B. & Ringach, D.L. Link between orientation and retinotopic maps in primary visual cortex. *Proc. Natl. Acad. Sci. USA* **109**, 7091 (2012).
16. Ringach, D.L. On the origin of the functional architecture of the cortex. *PLoS ONE* **2**, e251 (2007).
17. White, L.E. & Fitzpatrick, D. Vision and cortical map development. *Neuron* **56**, 327 (2007).
18. Seung, H.S. & Sompolinsky, H. Simple models for reading neuronal population codes. *Proc. Natl. Acad. Sci. USA* **90**, 10749 (1993).
19. Ma, W.J., Beck, J.M., Latham, P.E. & Pouget, A. Bayesian inference with probabilistic population codes. *Nat. Neurosci.* **9**, 1432 (2006).
20. Graf, A.B., Kohn, A., Jazayeri, M. & Movshon, J.A. Decoding the activity of neuronal populations in macaque primary visual cortex. *Nat. Neurosci.* **14**, 239 (2011).
21. Paradiso, M.A. A theory for the use of visual orientation information which exploits the columnar structure of the striate cortex. *Biol. Cybern.* **58**, 35 (1988).
22. Chen, Y., Geisler, W.S. & Seidemann, E. Optimal decoding of correlated neural population responses in the primate visual cortex. *Nat. Neurosci.* **9**, 1412 (2006).
23. De Valois, R.L., Albrecht, D.G. & Thorell, L.G. Spatial frequency selectivity of cells in macaque visual cortex. *Vision Res.* **22**, 545 (1982).
24. Ringach, D.L. Spatial structure and symmetry of simple-cell receptive fields in macaque primary visual cortex. *J. Neurophysiol.* **88**, 455 (2002).
25. Webster, M.A. & De Valois, R.L. Relationship between spatial-frequency and orientation tuning of striate-cortex cells. *J. Opt. Soc. Am. A* **2**, 1124 (1985).
26. Grinvald, A. & Hildesheim, R. VSDI: a new era in functional imaging of cortical dynamics. *Nat. Rev. Neurosci.* **5**, 874 (2004).
27. Van Essen, D.C., Newsome, W.T. & Maunsell, J.H. The visual field representation in striate cortex of macaque monkey: asymmetries, anisotropies, and individual variability. *Vision Res.* **24**, 429 (1984).
28. McIlwain, J.T. Point images in the visual system: new interest in an old idea. *Trends Neurosci.* **9**, 354 (1986).
29. Palmer, C.R., Chen, Y. & Seidemann, E. Uniform spatial spread of population activity in primate parafoveal V1. *J. Neurophysiol.* **107**, 1857 (2012).
30. Polat, U., Mizobe, K., Pettet, M. & Kasamatsu, T. Collinear stimuli regulate visual responses depending on cell's contrast threshold. *Nature* **391**, 580–584 (1998).
31. Polat, U. & Sagi, D. Lateral interactions between spatial channels: suppression and facilitation revealed by lateral masking experiments. *Vision Res.* **33**, 993 (1993).
32. Williams, C.B. & Hess, R.F. Relationship between facilitation at threshold and suprathreshold contour integration. *J. Opt. Soc. Am. A Opt. Image Sci. Vis.* **15**, 2046–2051 (1998).
33. Duncan, R.O. & Boynton, G.M. Cortical magnification within human primary visual cortex correlates with acuity thresholds. *Neuron* **38**, 659 (2003).
34. Schwarzkopf, D.S., Song, C. & Rees, G. The surface area of human V1 predicts the subjective experience of object size. *Nat. Neurosci.* **14**, 28 (2011).
35. Fang, F., Boyaci, H., Kersten, D. & Murray, S.O. Attention-dependent representation of a size illusion in human V1. *Curr. Biol.* **18**, 1707 (2008).
36. Murray, S.O., Boyaci, H. & Kersten, D. The representation of perceived angular size in human primary visual cortex. *Nat. Neurosci.* **9**, 429–434 (2006).
37. Motter, B.C. Central V4 receptive fields are scaled by the V1 cortical magnification and correspond to a constant-sized sampling of the V1 surface. *J. Neurosci.* **29**, 5749 (2009).
38. Harvey, B.M. & Dumoulin, S.O. The relationship between cortical magnification factor and population receptive field size in human visual cortex: Constancies in cortical architecture. *J. Neurosci.* **31**, 13604 (2011).
39. Dumoulin, S.O. & Hess, R.F. Cortical specialization for concentric shape processing. *Vision Res.* **47**, 1608 (2007).
40. Hegd , J. & Van Essen, D.C. A comparative study of shape representation in macaque visual areas v2 and v4. *Cereb. Cortex* **17**, 1100 (2007).
41. Pasupathy, A. & Connor, C.E. Population coding of shape in area V4. *Nat. Neurosci.* **5**, 1332 (2002).
42. Ito, M. & Komatsu, H. Representation of angles embedded within contour stimuli in area V2 of macaque monkeys. *J. Neurosci.* **24**, 3313–3324 (2004).
43. Teichert, T., Wachtler, T., Michler, F., Gail, A. & Eckhorn, R. Scale-invariance of receptive field properties in primary visual cortex. *BMC Neurosci.* **8**, 38 (2007).

ONLINE METHODS

Imaging subjects and stimuli. The results reported here are based on methods that have been described in detail previously^{22,44,45}. Here we focus on details that are of specific relevance to the current study. All procedures were approved by the University of Texas Institutional Animal Care and Use Committee and conform to US National Institutes of Health standards.

Three male adult monkeys (*Macaca mulatta*) were trained to maintain fixation while a small stationary Gabor or plaid stimulus was presented on a uniform gray background. Each trial began when the monkey fixated on a small spot of light (0.1 degrees) on a CRT display. Following an initial fixation, the sine-phase Gabor stimulus ($\sigma = 0.167^\circ$, $f = 2$ cpd or 4 cpd) was flashed at 5 Hz for 1,000 ms (60 ms on, 140 ms off) at a visual eccentricity between 2.40 and 3.82 degrees. To minimize the risk that monkeys would shift their gaze toward or away from the stimulus, a second, identical Gabor stimulus was simultaneously presented in the opposite quadrant of the visual field. Throughout the trial, the monkey was required to maintain gaze in a small window ($<2^\circ$ full width) around the fixation point to obtain a reward. The contrast of the stimulus was 100% at a mean luminance of 30 cd m⁻². The display had a resolution of 1,024 × 768 pixels and a 100-Hz refresh rate. In each session, trials representing different visual stimulus conditions, including blank trials, were randomly interleaved.

Selection of stimulus parameters. We used stimulus spatial frequencies of 2 and 4 cpd despite the fact that our V1 model predicted larger reductions in the effect of carrier orientation on cortical aspect ratio, and thus larger experimental effects, for stimuli composed of higher spatial frequency carriers. Our decision to use the 4-cpd stimuli for the high spatial-frequency condition was motivated primarily by concerns about the quality of signals in the imaging experiments. At the eccentricities represented in our VSDI recording chambers (2–4 degrees), the response was strongest to 2-cpd stimuli and dropped rapidly as the spatial frequency increased. Thus, in addition to changing the aspect ratio of the response, using Gabors composed of higher spatial frequency carriers reduced both the amplitude and the signal-to-noise ratio of the VSDI responses so that fits to the spatial envelope of the response became unreliable. We selected the 4-cpd stimuli as a compromise to simultaneously maximize both the experimental effect size and the signal-to-noise ratio.

Analysis of the imaging data. Imaging data were collected at 110 Hz at a resolution of 512 × 512 pixels. The size of each pixel was approximately 32 × 32 μm². Our basic analysis was divided into four steps. First, we normalized the responses at each pixel by the average fluorescence at that pixel across all trials and frames. Second, we removed from each pixel a linear trend estimated on the basis of the response in the 100-ms interval before stimulus onset for each trial. Third, we removed trials with aberrant VSDI responses (generally fewer than 1% of the trials⁴⁵). Finally, we subtracted the average response to the blank condition from the stimulus-present conditions.

After this analysis, the spatial properties of the responses in each trial were determined. First, we computed the amplitude of the 5-Hz response at each location in the fluorescence image. Then we averaged these response amplitudes across all trials in a particular stimulus condition and experimental session. Finally, for each condition, we computed the center, orientation, amplitude and aspect ratio of the best-fitting (in a least-squares sense) two-dimensional Gaussian function of the following form:

$$g(x, y) = A \exp\left(\frac{x'^2}{2\sigma_{x'}^2} - \frac{y'^2}{2\sigma_{y'}^2}\right) \quad (1)$$

$$\begin{cases} x' = (x - \mu_x)\cos\theta - (y - \mu_y)\sin\theta \\ y' = (x - \mu_x)\sin\theta + (y - \mu_y)\cos\theta \end{cases}$$

In analyzing each experiment, the Gaussian location (μ_x , μ_y) and orientation (θ) parameters were fit to all conditions and held fixed across conditions. Effectively, this meant that the major axis of the Gaussian was aligned with the direction maximizing the cortical magnification. Results from sessions that included retinotopic-mapping blocks indicated that this direction was generally within 5 degrees of the direction corresponding to the visual vertical axis. Retinotopic maps (Fig. 3b) were obtained using a previously described method⁹. Normalized physiological aspect ratios were computed by taking the physiological

aspect ratio for each carrier condition (σ_y / σ_x) and dividing by the average aspect ratio across conditions. We computed standard errors on the aspect ratio in each condition and session using a jackknife technique. We combined these estimates to compute the maximum-likelihood aspect ratio and the associated standard errors and confidence intervals across sessions. These values (the maximum likelihood aspect ratios and associated standard errors) were used in computing the reported statistical tests.

Effects of fixational eye movements. Small fixational eye movements could potentially give rise to elongated responses such as those reported here if they were systematically correlated with the orientation of the carrier grating. To test for such an effect, we quantified the eye movements in each trial by computing the horizontal (σ_x) and vertical (σ_y) s.d. of eye position during the stimulus presentation (Supplementary Fig. 3). We then ran two *t* tests to determine whether either of these measures varied systematically as a function of the carrier orientation. These tests indicated that neither the s.d. along the horizontal direction ($t_{102} = 0.015$, $P = 0.99$) nor the s.d. along the vertical direction ($t_{102} = 0.270$, $P = 0.79$) varied significantly as a function of Gabor carrier orientation.

Relationship between VSDI signals and population spiking activity. An important question in considering the implications of measured VSDI signals for perception is what is the relationship between the VSDI signals that we observed and the spiking activity that was accessible to the downstream visual and decision areas that contributed more directly to behavior. Recent results⁴⁶ suggest that the VSDI signal is dominated by subthreshold activity and that the spiking activity of the neural population can be represented approximately as a power function of the VSDI responses. Because a Gaussian function raised to a power N is still a Gaussian function (with a space constant σ that is smaller by a factor of \sqrt{N}), the spiking responses of a neural population whose VSDI responses are described by a two-dimensional Gaussian with space constants of σ_H in the horizontal direction and σ_V in the vertical direction could be described by a two-dimensional Gaussian with space constants σ_H / \sqrt{N} and σ_V / \sqrt{N} . In other words, the population spiking responses should have an aspect ratio similar to that of the VSDI responses, but a reduced overall extent.

Psychophysical subjects and stimuli. Ten human subjects (eight naive undergraduates, 4 male and 4 female, and two experienced psychophysical observers, both males, who were naive to the aims of the study) with normal or corrected-to-normal vision participated in this study. All human subjects provided informed consent, and the procedures were approved by the University of Texas Institutional Review Board. Stimuli were grayscale images presented on a calibrated CRT monitor located 70 cm from observers and set to a resolution of 1,280 × 1,024 pixels (pixel size = 0.27 × 0.27 mm). Each stimulus display consisted of a pair of targets, each positioned 2.5 degrees from fixation and centered in opposing quadrants of the display, so that one of the stimuli always appeared on the left and one on the right. The target stimuli were horizontal, vertical and plaid 2-cpd gratings (4 cpd in the high frequency conditions) windowed by a two-dimensional Gaussian contrast function whose s.d. in the vertical and horizontal direction had a geometric average of 0.167 degrees. All stimuli were presented at 80% contrast against a uniform gray background with a mean luminance of 40 cd m⁻².

Shape judgment task. Before each trial, the observer fixated a dot at the center of the display and initiated the trial with a button press. The fixation point dimmed immediately and, a random time (150–350 ms) later, the two target stimuli appeared for 200 ms. The observer's task was to determine which of the two targets (left-side or right-side) had the more circular contrast envelope (that is, the target whose spatial extent was more circular). In each pair of targets, one (the standard) was a plaid stimulus, whereas the other (the comparison) could be either a plaid, horizontal or vertical stimulus. The location of the standard (that is, left or right) was selected randomly, as were the pair of quadrants (that is, upper left and lower right or upper right and lower left) in which the stimuli were presented and the phases of the carrier gratings. The standard stimulus took on five discrete aspect ratio values (0.67, 0.82, 1.0, 1.22, 1.50) spaced evenly along a log axis. The value of the comparison stimulus on each trial was chosen on a uniform interval ± 1 log (base 2) unit from the aspect ratio of the standard.

All observers completed five sessions of the experiment. Each session began with a practice block in which the standard and comparison stimuli were both

plaids and subjects received auditory feedback on each trial. After the practice block was completed, subjects ran 4 blocks of 300 experimental trials each without feedback. High and low spatial-frequency blocks were interleaved and their order counterbalanced across observers.

Analysis of psychophysical data. The purpose of the psychophysical task was to determine whether the perceived shape of the Gabor stimuli varied systematically with the orientation of the carrier grating, as we hypothesized based on the physiological measurements. Our prediction was that, relative to a neutral (plaid) stimulus, a Gabor would appear stretched along the orientation of the bars composing its carrier grating. For example, a vertical Gabor should appear vertically stretched, whereas a horizontal Gabor should appear horizontally stretched.

To measure this effect, we determined the point of subjective equality, the scaling adjustment required to make the aspect ratio of the Gabor comparison stimulus perceptually equivalent to that of the plaid standard. Note that this adjustment should exactly counter the perceptual effect. For example, if a circular vertical Gabor ($AR = 1.0$) were perceived as having a vertical-to-horizontal aspect ratio of 1.5, then to appear circular, its aspect ratio would have to be $1/1.5$. The point of subjective equality β_c is therefore equal to the reciprocal of the perceptual effect. We estimated the point of subjective equality by determining the maximum likelihood value of β_c , using a psychophysical task.

To determine the value of β_c , we assumed that observers make their decisions based on noisy perceptual estimates of the aspect ratios of the comparison (AR_c) and the standard (AR_s) stimuli. The noise associated with each of these estimates was assumed to be proportional to the aspect ratio and distributed log normally.

That is,

$$\begin{aligned} \log_2(AR_s) &= X_s \sim N(\mu_s, \sigma) \\ \log_2(AR_c) &= X_c \sim N(\mu_c - \log_2(\beta_c), \sigma) \end{aligned} \quad (2)$$

where μ_s is the veridical (log) aspect ratio of the standard stimulus, and μ_c is the veridical (log) aspect ratio of the comparison stimulus. This assumption is equivalent to assuming Weber's law behavior for aspect ratios, which seems to hold approximately for the relatively small aspect ratios used here⁴⁷. Furthermore, the estimates of the point of subjective equality are not strongly dependent on the assumed form of the noise.

The task is to determine which stimulus is more circular, which is equivalent to determining which of the two log aspect ratios is closer to zero. In other words, the observer selects the standard whenever $X_s^2 < X_c^2$ and chooses the comparison otherwise. In the simplest case, we can compute the probability of choosing the standard as

$$p(X_s^2 < X_c^2 | \mu_s, \mu_c, \sigma, \beta_c) = \int_{-\infty}^{\infty} p(X_s^2 < x_c^2 | \mu_s, \sigma) p(x_c^2 | \mu_c, \sigma, \beta_c) dx_c \quad (3)$$

where $p(X^2 | \mu, \sigma)$ is a non-central chi-squared distribution with one degree of freedom and non-centrality parameter $\lambda = (\mu^2 / \sigma^2)$. The analytic properties of this distribution, along with approximations of the associated cumulative distribution function $p(X^2 < x | \mu, \sigma)$ have been characterized elsewhere⁴⁸.

In this simple case, the PSE occurs when the observer is equally likely to choose the standard or the comparison stimulus. PSE's for two alternative forced-choice tasks are usually determined by finding the value of the comparison for which the probability of choosing the standard is 50%. However, when the standard can be physically distinguished from the comparison using features irrelevant to the task, PSE's estimated using the 50% point can be confounded with response bias⁴⁹.

In our psychophysical experiment, the carrier of the standard target was always a plaid, whereas the comparison was usually an oriented Gabor. Thus, the observer could usually determine which of the two stimuli the standard was. Observers exhibited a systematic response bias, favoring the standard when the aspect ratios were perceptually indistinguishable and even when the comparison stimulus was perceived as slightly more round than the comparison.

This bias is evident in the psychometric functions plotted in **Figure 6c**. The reversals in individual curves from a decreasing slope to an increasing slope indicate the perceived transition of the comparison from a horizontally oriented to a vertically oriented shape, with points of zero slope indicating perceived circularity. If observers responded in an unbiased way, then at these points of

perceived circularity the probability of choosing the standard should be at most 0.5. Instead, in **Figure 6c** these points always occur at values greater than 0.5, indicating a response bias.

To account for this response bias, we introduced the adjusted guessing rate parameter γ , reflecting the observers overall bias toward choosing the standard as the most circular of the stimuli. Formally, γ represents the observer's prior probability on the standard stimulus.

Applying this prior using Bayes' rule and solving for $p(\text{standard}) = p(\mu_s < \mu_c - \log_2(\beta_c))$ yields

$$p(\text{standard} | \mu_s, \mu_c, \sigma, \beta_c) = \frac{\gamma p(X_s^2 < X_c^2 | \mu_s, \mu_c, \sigma, \beta_c)}{\gamma p(X_s^2 < X_c^2 | \mu_s, \mu_c, \sigma, \beta_c) + (1 - \gamma) p(X_s^2 > X_c^2 | \mu_s, \mu_c, \sigma, \beta_c)} \quad (4)$$

For trials in which the comparison and the standard were both plaids (and thus physically indistinguishable), the value of this parameter was 0.5 ($\gamma = 0.5$). Generally however, observers were biased toward choosing the standard as more circular ($\gamma > 0.5$). Note that because the design of the task allowed more extreme aspect ratios for the comparison stimuli (chosen from a symmetric log-scale interval around the standard) than for the standard stimuli, the empirical probability of the standard being the more circular of the two stimuli in our experiment was actually 0.67 and therefore the response bias exhibited by the observers is sensible.

In fitting the psychometric functions, we used the form in (equation (4)), except that we assumed a small fixed lapse rate of 1% to keep rare lapse errors from dominating the maximum likelihood fit, and we introduced a fourth parameter, β_s , to account for any overall tendency to perceive round stimuli as elongated (as might be caused by a small geometric anisotropy in the display). This parameter simultaneously added a fixed offset to the veridical log aspect ratios of the standard (μ_s) and the comparison (μ_c). We estimated the four free psychometric parameters $\{\sigma, \gamma, \beta_c, \beta_s\}$ simultaneously by pooling the response data across human observers and finding the maximum likelihood fit across all values of the standard. Separate fits were obtained for each comparison carrier condition (for example, plaid, horizontal grating, vertical grating), and 95% confidence intervals were estimated via bootstrapping using a case-resampling procedure with 1,000 repetitions.

Finally, our results did not depend critically on the details of this psychometric model. For example, although the dot markers in **Figure 6c** and **Supplementary Figure 2a**, which represent log-space binned averages of the human responses (the raw data at each point was a binary response) show that the data were well fit by the psychometric model (solid lines), the shifts in PSEs shown for the vertical and horizontal carriers in **Figure 6c** are evident even in the averaged human responses.

Simulating population responses. We simulated V1 responses within a $2^\circ \times 2^\circ$ patch of the visual field using 10,000 unique receptive field parameters (see below). Briefly, each complex cell's receptive field was represented by the nonlinear combination of a pair of Gabor functions in quadrature phase. In addition, each unique receptive field tiled the simulated visual field patch along a 101×101 rectangular array, so that each location in the grid was associated with the responses of 10,000 unique receptive fields centered on that location. The spatial distribution of complex cell responses was convolved with a Gaussian kernel to simulate the effect of receptive field position scatter that occurs at any given location in the visual cortex.

The specific steps of the simulation were as follows. First, for each cell in the population, we construct two Gabors, one in sine phase (g_s) and one in cosine phase (g_c), from the sampled frequency, height, width and orientation parameters. Second, to simulate the response of a complex cell to a particular stimulus, we take the sum of squares of the dot products each of the quadrature pair of Gabors⁵⁰ with the stimulus; that is, $r(x, y) = [g_s(x, y) \cdot I]^2 + [g_c(x, y) \cdot I]^2$. This is equivalent to computing the sum of the half-squared outputs of four Gabor-shaped simple cell receptive fields, each shifted from the next in 90° increments of phase. Third, for each set of cell parameters, we simulate a the stimulus-elicited responses \mathbf{R} of a population of cells with identical parameters, but different receptive field locations representing a 2×2 degree portion of the visual field, such that $\mathbf{R}_{ij} = r(x_j, y_i)$. Fourth, to simulate scatter in receptive field positions, we convolve

the result with a Gaussian kernel whose variance is set to match the variance of the receptive field center positions at a point in cortex (or, equivalently, the variance of the cortical positions of cells with receptive fields centered on the same point in visual space).

$$\mathbf{B}_l = \mathbf{R}_l \otimes K(\sigma_{PS}(l)) \quad (5)$$

where $\sigma_{PS}(l)$ is the scatter associated with the l th receptive field. Physiological measurements in monkey⁵¹ and cat⁵² suggest that the average scatter in receptive field centers at a particular location in V1 is about 50% of the average receptive field size, which is what we assume in our model. Preliminary results from our lab (data not shown) suggest that the size of the cortical point image (CPI) for Gabor stimuli sharing a common envelope size is approximately constant across carriers of different spatial frequency, suggesting that the population receptive field (pRF) does not change as a function of spatial frequency²⁹. To account for these results, we assume that the scatter of receptive field centers increases as a function of spatial frequency (that is, that smaller receptive fields have more scatter than larger receptive fields centered on the same cortical location). This is effectively equivalent to assuming a uniform tiling of visual space for each of our receptive field sizes. Relaxing this assumption (for example, assuming a fixed scatter) does not significantly affect our predictions regarding aspect ratios, but it predicts that response spread should decrease with increasing spatial frequency. To implement this relationship, we vary the scatter associated with each receptive field such that the sum of the positional scatter variance $\sigma_{PS}^2(l)$ and the receptive field envelope variance $\sigma_{RF}^2(l)$ remains constant; that is, $\sigma_{PS}^2(l) = \max(\sigma_{PS}^2 + \sigma_{RF}^2 - \sigma_{RF}^2(l), 0)$. Finally, at each location, the final response (across all receptive fields) is simply the average of the responses to the individual receptive fields

$$\mathbf{E} = \frac{1}{N} \sum_i^N \mathbf{B}_i \quad (6)$$

Sampling receptive field parameters. Peak spatial frequency tuning parameters were estimated from existing electrophysiological data²³ measured from cells with receptive field centers falling between 3 and 5 degrees in the visual periphery. A log Gaussian ($\mu = 2.34$ cpd, $\sigma = 2.01$ octaves) was fitted to the combined histograms.

The distributions of receptive field shape parameters were obtained by combining data from a more recent study²⁴ that provides simple-cell width and length parameters in period units (that is, $n_x = \sigma_x f_x$, $n_y = \sigma_y f_x$), and those from an older study²³ that provides orientation and spatial frequency bandwidth parameters.

To use common parameters, the bandwidth parameters from the older study⁴⁷ were transformed as

$$n_x = \frac{\sqrt{\ln(4)} 2^{W_{SF}} + 1}{2\pi} \frac{2^{W_{SF}} + 1}{2^{W_{SF}} - 1}, n_y = \frac{\sqrt{\ln(4)}}{2\pi \tan(W_O/2)} \quad (7)$$

where W_{SF} represents the spatial frequency bandwidth in octaves and W_O represents the orientation bandwidth. In addition, sample receptive field parameters were excluded if they led to undefined spatial frequency bandwidths or if they had extremely large orientation bandwidths (that is, $W_O > 180^\circ$).

Unfortunately, although one study²³ shows that a cell's spatial frequency bandwidth varies systematically with its peak spatial frequency, the receptive field shape data in both studies cited above was reported in a spatial frequency-independent manner. Mean spatial frequency bandwidth decreases approximately linearly with the log of the peak spatial frequency (slope = -0.246 , intercept = 1.779). To account for this trend when sampling receptive field shape for a cell with a particular peak spatial frequency, we first computed a function $q(W_{SF})$ representing the distribution of spatial frequency bandwidths in our distribution of sample receptive fields. This function was obtained as the maximum-likelihood gamma distribution function fit to the octave bandwidths. Second, we computed $p(W_{SF} | f)$, the (Gaussian) distribution of bandwidths expected for a given frequency from the previously reported empirical relationship²³. Third, we sampled receptive fields from a multinomial distribution where the probability of choosing each receptive field was weighted by $p(W_{SF} | f)/q(W_{SF})$ and W_{SF} represents the receptive field's spatial frequency octave bandwidth.

To sample the set of receptive field parameters for a single V1 neuron, we first sampled a spatial frequency from the first distribution, then sampled a receptive field shape from the second and third distributions, and finally sampled the orientation from a uniform distribution. To obtain a population of receptive field parameters for cells centered at a particular location, we simply repeated this process. A summary of the resulting distribution of receptive field parameters is shown in **Supplementary Figure 1**. The average simulated receptive field had a peak spatial frequency tuning of 2.98 cpd, and bandwidth of 1.6 octaves, and a space constant (σ_{RF}) of 0.26° . Because the average simulated receptive field positional scatter (σ_{PS}) was half the width of the average receptive field, the resulting pRF had a space constant of about 0.29° .

Limitations of the population response model. It is important to point out that our estimates of V1 parameters are informed and limited by the measurements available in the literature. Consequently, our simulations are only intended to provide qualitative predictions of the physiological and perceptual responses. The precise perceived and physiological aspect ratios for a particular stimulus depend on the amount of scatter in receptive field center locations, the exact form of the simple-cell response nonlinearity and the distribution of receptive field shapes, which have not been measured precisely and may vary somewhat from one cortical location to another, from an individual animal to another and certainly from one species to another.

Additional simulations (data not shown), in which we varied the receptive field parameter distributions, receptive field scatter and the exponent of the simple-cell nonlinearity, resulted in small quantitative, but not qualitative, differences in our results, confirming that our main predictions—that population responses in V1 are systematically elongated for Gabors matching the average spatial frequency and bandwidth parameters of V1 neurons and that this elongation effect is attenuated for more poorly matching stimuli—are robust to minor variations in the specific population parameters used in the simulation.

Statistical analysis. All error bars represent 95% bootstrap-computed confidence intervals for the mean and statistical significance was determined using two-sided t tests, with conservative estimates of the effective degrees of freedom. For the physiological data, jackknife estimates of standard error were computed across all trials (ten trials per condition per session) and the effective degrees of freedom were determined by the number of experimental sessions. For the psychophysical data, standard error was estimated from the bootstrap-computed 95% confidence intervals and the effective degrees of freedom were determined by the number of individual subjects. No statistical methods were used to pre-determine sample sizes, but our sample sizes were similar to those reported in previous publications in the field^{2,12,45,46}. Data distribution was assumed to be normal, but this was not formally tested. However, the bootstrap-computed confidence intervals accurately reflect the empirical data distributions and can be used to aid interpretation.

44. Seidemann, E., Arieli, A., Grinvald, A. & Slovin, H. Dynamics of depolarization and hyperpolarization in the frontal cortex and saccade goal. *Science* **295**, 862 (2002).
45. Chen, Y., Geisler, W.S. & Seidemann, E. Optimal temporal decoding of neural population responses in a reaction-time visual detection task. *J. Neurophysiol.* **99**, 1366 (2008).
46. Chen, Y., Palmer, C.R. & Seidemann, E. The relationship between voltage-sensitive dye imaging signals and spiking activity of neural populations in primate V1. *J. Neurophysiol.* **107**, 3281 (2012).
47. Nachmias, J. Shape and size discrimination compared. *Vision Res.* **51**, 400 (2011).
48. van Aubel, A. & Gawronski, W. Analytic properties of noncentral distributions. *Appl. Math. Comput.* **141**, 3 (2003).
49. Morgan, M., Dillenburger, B., Raphael, S. & Solomon, J.A. Observers can voluntarily shift their psychometric functions without losing sensitivity. *Atten. Percept. Psychophys.* **74**, 185 (2012).
50. Adelson, E.H. & Bergen, J.R. Spatiotemporal energy models for the perception of motion. *J. Opt. Soc. Am. A* **2**, 284 (1985).
51. Dow, B.M., Snyder, A., Vautin, R. & Bauer, R. Magnification factor and receptive field size in foveal striate cortex of the monkey. *Exp. Brain Res.* **44**, 213 (1981).
52. Hetherington, P.A. & Swindale, N.V. Receptive field and orientation scatter studied by tetrode recordings in cat area 17. *Vis. Neurosci.* **16**, 637 (1999).